Research Article | Vol. 11, No. 8 / 1 August 2020 / Biomedical Optics Express 4800
Biomedical Optics EXPRESS

Waveguide-based surface-enhanced Raman spectroscopy detection of protease activity using non-natural aromatic amino acids

NINA TURK,[1,2,*] ALI RAZA,[1,2,3] PIETER WUYTENS,[1,2,4] HANS DEMOL,[5,6] MICHIEL VAN DAELE,[7] CHRISTOPHE DETAVERNIER,[7] ANDRE SKIRTACH,[2,8] KRIS GEVAERT,[5,6] AND ROEL BAETS[1,2]

[1] *Photonics Research Group, Ghent University – IMEC, Technologiepark 126, 9052 Ghent, Belgium*
[2] *Center for Nano- and Biophotonics, Ghent, Belgium*
[3] *Currently with Microsoft, Keilalahdentie 2-4, 02150 Espoo, Finland*
[4] *Currently with IMEC, Kapeldreef 75, 3001 Heverlee, Belgium*
[5] *VIB-UGent Center for Medical Biotechnology, Ghent, Belgium*
[6] *Department of Biomolecular Medicine, Ghent University, Belgium*
[7] *Department of Solid State Sciences, CoCooN Research Group, Ghent University, Belgium*
[8] *Department of Biotechnology, Ghent University, Belgium*
[*] *nina.turk@ugent.be*

Abstract: Surface enhanced Raman spectroscopy (SERS) is a selective and sensitive technique, which allows for the detection of protease activity by monitoring the cleavage of peptide substrates. Commonly used free-space based SERS substrates, however, require the use of bulky and expensive instrumentation, limiting their use to laboratory environments. An integrated photonics approach aims to implement various free-space optical components to a reliable, mass-reproducible and cheap photonic chip. We here demonstrate integrated SERS detection of trypsin activity using a nanoplasmonic slot waveguide as a waveguide-based SERS substrate. Despite the continuously improving SERS performance of the waveguide-based SERS substrates, they currently still do not reach the SERS enhancements of free-space substrates. To mitigate this, we developed an improved peptide substrate in which we incorporated the non-natural aromatic amino acid 4-cyano-phenylalanine, which provides a high intrinsic SERS signal. The use of non-natural aromatics is expected to extend the possibilities for multiplexing measurements, where the activity of several proteases can be detected simultaneously.

1. Introduction

Proteases are enzymes that catalyze the hydrolysis of peptide bonds. They play an important role in many signaling pathways and are important actors in several human diseases, including inflammation, infectious diseases, cancer and degenerative diseases [1,2]. As such, proteases are extremely interesting as drug targets and protease inhibitors are used as drugs to treat cardio-vascular diseases [3] and HIV infection [4] amongst others. Such inhibitors are generally small molecules that block the active site of a protease, thereby suppressing its activity [1]. In drug development, sensitive analysis of protease activity is of crucial importance since it allows to identify protease inhibitors, which efficiently block protease activity. As almost 600 proteases have been identified in the human genome [5], there is also a clear need for a selective, sensitive and multiplexed method of measuring protease activities.

In the past decades, colorimetric assays and liquid chromatography have been widely used. However, these do not offer a high sensitivity or multiplexing capabilities [6]. In recent years, different strategies based on nanoparticle-peptide complexes used fluorescence to detect protease

#398038 https://doi.org/10.1364/BOE.398038
Journal © 2020 Received 19 May 2020; revised 22 Jul 2020; accepted 22 Jul 2020; published 31 Jul 2020

Biomedical Optics EXPRESS

activity, offering high sensitivity measurements both *in vitro* and *in vivo* [7,8]. Such fluorescence-based techniques however provide limited multiplexing possibilities [7]. On the other hand, Raman spectroscopy enables spectrally multiplexed measurements due to the specificity of Raman spectra [9]. Surface-Enhanced Raman Spectroscopy (SERS) can be used to enhance the inherently weak Raman signal in close proximity of metallic nanostructures [10]. The typical sizes of the plasmonic hotspots used in SERS match well with the nanometer-sized peptides recognized and cleaved by proteases. This makes SERS an attractive method for sensing of protease activities, which can be detected via dispersion or aggregation of SERS nanoparticles in the presence of proteases [11,12,13,14]. Uncontrolled aggregation of metal nanoparticles can however create reproducibility issues. To overcome these, the peptide can be immobilized on a well-controlled SERS structure and then specifically cleaved by a protease [15,16]. This allows a reproducible, quantitative approach of great interest for protease activity sensing.

A variety of SERS structures enabling high and reproducible SERS enhancements has been developed [17]. However, these structures typically rely on bulky and expensive instrumentation such as confocal Raman microscopes, which largely limits their use to laboratory environments. There has been a push for portable miniaturized devices, which can perform sensitive and accurate spectroscopic detection. An integrated photonics approach can offer the solution by bringing various free-space optical components to a single chip. Their integration leads to devices that are robust, cheap, mass-reproducible and reliable, and additionally allows parallelism [18]. In recent years, the silicon nitride (Si_3N_4) platform was developed, which enables waveguide-based excitation and collection of Raman [19,20,21,22] and SERS spectra [23,24,25,26,27,28,29,30,31]. Despite the continuous improvement in the performance of the waveguide-based SERS platforms, they are limited by the background signal of the Si_3N_4 [32,33]. Currently, free-space SERS substrates still slightly outperform waveguide-based SERS platforms [34]. Nevertheless, with ongoing development, integrated Raman platforms are becoming increasingly interesting for biological applications as they enable an integrated lab-on-a-chip approach [35].

In this work, we used the nanoplasmonic slot waveguide to demonstrate waveguide-based SERS detection of trypsin activity via the cleavage of peptide substrate. The concept of free-space SERS detection of protease activity was previously demonstrated on gold nanodomes for the detection of trypsin activity through the SERS spectra of surface-bound peptides consisting of only natural amino acids [16]. However, due to the poorer SERS performance of the nanoplasmonic slot waveguide compared to free-space gold nanodomes, just the natural aromatic acids do not provide sufficient SERS signal for waveguide-based detection [36]. We therefore developed an improved peptide substrate using the non-natural aromatic amino acid 4-cyano-phenylalanine [37]. Here, we report that non-natural aromatics can be used as SERS reporters when incorporated in a peptide which is then successfully cleaved by trypsin, both in bulk solution as well as when bound on the SERS substrate. Considering that only the three natural aromatic amino acids, namely phenylalanine, tyrosine and tryptophan, provide a relatively high SERS signal [38], the use of non-natural aromatics significantly extends the possibilities of multiplexing measurements, where the activity of several proteases is simultaneously detected. In the end, we used the peptide with the incorporated non-natural aromatic to show waveguide-based SERS detection of trypsin activity, paving the way towards SERS-based monitoring of protease activity on an integrated lab-on-a-chip platform.

2. SERS-based sensing of protease activity

2.1. Concept of SERS-based sensing of protease activity

SERS-based protease activity sensing relies on monitoring cleavage of peptide substrates, and it is shown schematically in Fig. 1. The selected SERS substrate is labelled with a peptide substrate for trypsin, our model protease. We have fabricated a specific peptide substrate for trypsin with the amino acid sequence NH_2-CALNN(CN-F)GSG(CN-F)GGGGVRGNFSF-COOH, where

Biomedical Optics EXPRESS

each letter represents a natural amino acid and CN-F represents the non-natural aromatic amino acid 4-cyano-phenylalanine. The peptide contains a cysteine (C) that allows it to covalently bind to the gold nanostructure, which provides the SERS enhancement [39], with the peptide forming a monolayer on the gold surface [40]. The Raman signal of the peptide comes from the two aromatic amino acids, in our case 4-cyano-phenylalanine (CN-F), which provides the reference SERS peak at 1180 cm^{-1}, and phenylalanine (F) with a peak at 1003 cm^{-1}. Each aromatic amino acid appears in the sequence twice, so as to double their SERS signal strengths. Between the two aromatics, there is a specific cleavage site for trypsin, which cleaves the C-terminal to the arginine residue (R) [41]. After cleavage of the peptide, the short peptide fragment NH_2-GNFSF-COOH diffuses away from the gold surface, consequently reducing the intensity of the 1003 cm^{-1} peak in the SERS spectrum. The SERS peak originating from the CN-F is expected to stay constant and can thus serve as a normalization peak. The F and CN-F peak counts are integrated, and the F/CN-F peak intensity ratio is used as a metric for the efficiency of trypsin cleavage [16].

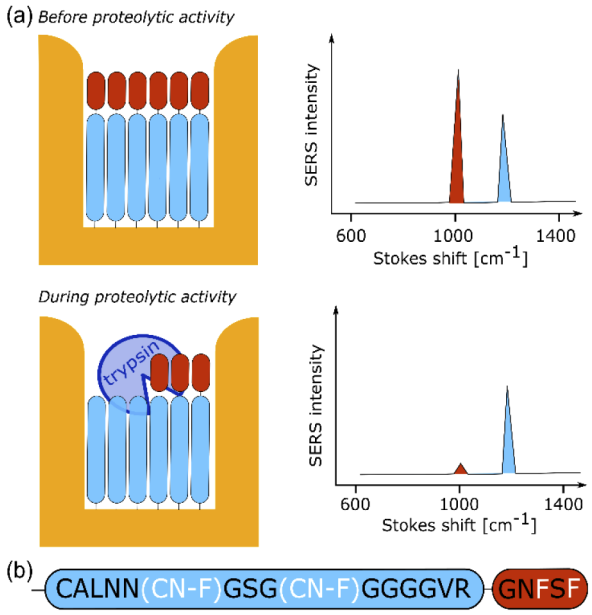

Fig. 1. **(a)** The concept of protease activity detection via peptide bond cleavage using SERS, where the SERS signal originates from the aromatic amino acids phenylalanine (F) and 4-cyano-phenylalanine (CN-F). The peptide forms a monolayer on the gold nanostructures and is then cleaved by a protease (here trypsin). As the cleaved-off part of the peptide diffuses away from the gold surface, the corresponding SERS peak intensity decreases. **(b)** Peptide substrate for trypsin, written with using the single-letter amino acid code. White letters represent the aromatic amino acids that provide SERS signals, namely phenylalanine (F) and the non-natural 4-cyano-phenylalanine (CN-F).

2.2. SERS substrates

The SERS experiments were performed using the free-space gold nanodomes and the waveguide-based nanoplasmonic slot waveguides, using a confocal Raman microscope. First, we used the gold nanodomes to establish that trypsin cleaves its peptide substrate with the incorporated non-natural aromatic, and that SERS can be used to detect such cleavage events. We then used the peptide with the non-natural aromatics to demonstrate SERS detection of trypsin activity on the integrated nanoplasmonic slot waveguide.

Biomedical Optics EXPRESS

Gold nanodomes (Fig. 2-top) provide high SERS enhancement, which mostly originates from the high field enhancement in the gaps of the nanodomes [16]. The smaller gaps enable higher SERS enhancements, but are less accessible to trypsin with a molecular weight of 23 kDa and a corresponding Stokes radius of 2-3 nm [42]. Gold nanodomes with gap sizes of 12 nm were shown to provide a good compromise between SERS enhancement and accessibility of trypsin to the gaps [16].

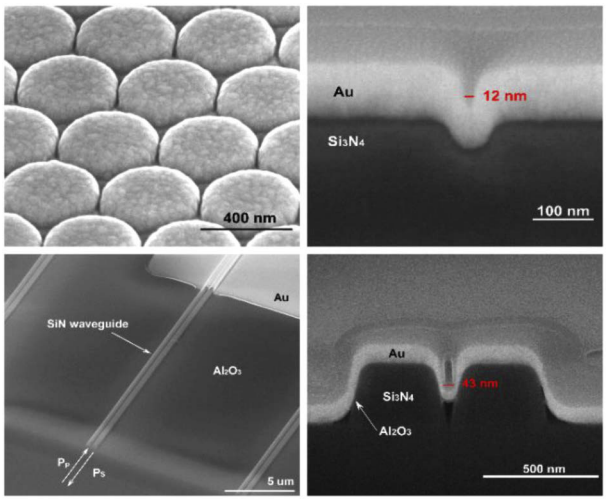

Fig. 2. (top) Gold nanodomes are free-space SERS substrate with an average gap size of 12 nm. **(bottom)** Waveguide-based nanoplasmonic slot waveguides have an average gap size of 43 nm.

Nanoplasmonic slot waveguides (Fig. 2-bottom) are the best performing waveguide-based SERS substrates to date, yet they are currently still outperformed by conventional free-space SERS substrates such a gold nanodomes [34]. On the other hand, nanoplasmonic slot waveguides offer the advantageous non-resonant enhancement and can be produced using scalable high-volume fabrication techniques in micro-electronic fabs. Their main advantage is however their waveguide-based nature, which means they can be integrated on a photonic integrated chip for a reproducible, reliable and cheap SERS sensor of the protease activity. As in gold nanodomes, the smaller gaps in the nanoplasmonic slot waveguide lead to a higher SERS enhancement, but less accessibility for trypsin. We conducted our experiments on waveguides with a plasmonic gap of 43 ± 5 nm. Currently, we still need to use the Raman confocal microscope to measure the SERS spectra of the nanoplasmonic slot waveguide. In the last years, several papers were published which explore how to implement the functionalities of the Raman microscope on an integrated photonic chip, including a III/V integrated laser [43], integrated filters [44], a waveguide-based collection region [19] and an on-chip spectrometer [45]. Further effort is however needed to ensure the compatibility of all the different components and integrate them on the same photonic chip.

3. Methods

3.1. Production of the peptide

Peptides were synthesized using standard solid-phase fluorenylmethyloxycarbonyl chloride (Fmoc) chemistry on a SyroI (Biotage) instrument. The synthesis was started on 25 µmol preloaded Fmoc-His (Trt) or Fmoc-Phe wang resin (Novabiochem). Amino acids were coupled in 4-fold excess using HOBT/HBTU activation. The peptides were cleaved with TFA containing phenol,

Biomedical Optics EXPRESS

triisopropylsilane and 5% water for 3 h. Then, peptides were precipitated with tributylmethyl ether and recovered by centrifugation at 2000x g. The ether washing/centrifugation step was repeated three times. The peptides were purified using a water/acetonitrile gradient elution on by using RP-HPLC on a RPC C18 column (Macherey-Nagel).

3.2. HPLC and mass spectrometry

Trypsin was dissolved in 50 mM ammonium bicarbonate buffer (pH = 7.8) to a concentration of 5 µg/ml. After the addition of the peptide (100 µg/ml), the solution was incubated for an hour at 37°C. 750 µl of the solution was injected on a C-18 reversed phase high-performance liquid chromatography column (Macherey-Nagel) and eluted by a water/acetonitrile gradient (Akta Purifier, GE). Matrix-assisted laser desorption/ionisation time-of-flight mass spectrometry (Bruker MALDI-TOF) was used to determine the molecular weight of the peptide fractions.

3.3. Fabrication of the gold nanodomes

Gold nanodomes were fabricated using a nanosphere lithography-based process, described in detail in Ref. [16]. Briefly, a 200 nm thick silicon nitride film (Si_3N_4) was deposited on top of a silicon wafer with a diameter of 4 inches. A colloidal solution of 450 nm polystyrene beads (microParticles GmbH) was spin-coated on the Si_3N_4 surface, forming a monolayer of hexagonally-close packed polystyrene beads. The polystyrene beads were thinned down in an oxygen plasma and the pattern of nanodomes was etched into the Si_3N_4 substrate by an anisotropic reactive-ion etch. The remains of the polystyrene beads were lifted off in dichloromethane and the wafers were cleaned in a piranha solution (H_2SO_4:H_2O_2, 3:1). Finally, a 2 nm thick titanium adhesion layer and a 130 nm thick gold layer were sputtered on the sample. The maximum SERS enhancement factor of the gold nanodomes for a single molecule was estimated to be 10^7 using 3D FDTD simulations [16].

3.4. Fabrication of the nanoplasmonic slot waveguide

Nanoplasmonic slot waveguides were fabricated using a combination of atomic layer deposition and deep UV photolithography, as described in detail in Ref. [27]. Firstly, 2.3 µm thick SiO_2 and 220 nm thick Si_3N_4 layers were deposited on a 200 µm silicon wafer. The Si_3N_4 slot waveguides were patterned with 193 nm deep UV optical lithography and then etched by a reactive-ion etch process. The resulting average slot width was 150 nm. To narrow down the slot width, the waveguides were uniformly coated with 58 nm Al_2O_3 using atomic layer deposition (ALD). After ALD, gold waveguides were defined using photolithography and a 2 nm titanium adhesion layer and a 120 nm thick layer of sputtered gold were deposited. The maximum SERS enhancement factor of the nanoplasmonic slot waveguide with a gap of 15 nm was predicted to be 1.5×10^7 for a single molecule [27]. Experimental comparison shows that gold nanodomes still outperform the nanoplasmonic slot waveguides with similar gap sizes, providing 3-times higher signal-to-background ratio and 15-times higher signal-to-noise ratio [34]. However, due to fabrication difficulties, the fabricated nanoplasmonic slot waveguide had a relatively large size of 43 nm. In the future, nanoplasmonic slot waveguide can be fabricated with smaller gaps, which should allow to achieve higher SERS enhancements.

3.5. Raman microscope

A WITec Alpha300R+ confocal Raman microscope, a 785 nm excitation diode laser (Toptica), and a UHTS 300 spectrometer using a −75°C cooled CCD camera (ANDOR iDus 401) was used. The objectives Zeiss W N-Achroplan/W 20x/0.5 and Zeiss W Plan-Apochromat 63×/1.0 were used for the measurements of the gold nanodomes and the nanoplasmonic slot waveguide respectively. A fiber with 100 µm diameter was used to transfer the signal to the spectrometer and also served as a pinhole.

Biomedical Optics EXPRESS

3.6. SERS experiments with peptides

The peptide was first dissolved in dimethylformamide (DMF) and then diluted to a concentration of 100 µg/ml in 10% acetonitrile/water. The SERS substrates were cleaned with acetone, isopropyl alcohol and DI water, and dried with a N_2 gun. The samples were treated with oxygen plasma, immersed overnight in the peptide solution, and then rinsed with deionized water to remove any peptides that did not covalently bind to the gold. The sample was placed in a Petri dish filled with 3 ml of 50 mM ammonium bicarbonate buffer (pH 7.8). The reference SERS spectra of the uncleaved peptide were acquired with the confocal Raman microscope. In the trypsin cleavage experiments, the SERS substrates were incubated with 5 µg/ml trypsin for an hour at 37°C, then rinsed with DI water and their SERS spectra measured. On the gold nanodomes, the SERS response was excited using 1 mW laser power before the microscope objective. 40x/0.5 Zeiss water immersion objective was used to acquire spectra on a spatially distributed map of 7×7 pixels in a 40×40 µm area with an integration time of 3 s on each point to avoid signal degradation upon laser illumination. For nanoplasmonic slot waveguide, a 1 mW laser power before the microscope objective and a 63×/1.0 Zeiss water immersion objective were used to acquire 10 consecutive SERS spectra with the integration time up to 60 s.

3.7. SERS data analysis

For the SERS measurements on the gold nanodomes, the SERS maps were exported to MATLAB and aberrant spectra were discarded using a variance-based filter. Then, the background of each individual spectrum was subtracted using a window-based filter fir1 in the high-pass configuration. The SERS spectrum was plotted as the average spectra of one map of 7×7 measurements. Peak intensities were calculated by integrating the peak counts at their respective positions and subtracting the background with a linear fit for the individual spectra.

For the SERS measurements on the nanoplasmonic slot waveguides, the data were analyzed with WITec Project Four software. After removal of cosmic rays, the background was fitted with a polynomial and subtracted. The integrated areas of F and CN-F peak areas were then calculated on the background-subtracted spectrum.

4. Results and discussion

4.1. In-solution trypsin cleavage of the peptide monitored via RP-HPLC and SERS spectroscopy

We first established that trypsin cleaves the peptide substrate containing the non-natural aromatic. Therefore, we performed in-solution trypsin cleavage of the peptide substrate, separated the peptide fragments by RP-HPLC, labelled them on the gold nanodomes and collected their SERS spectra, as described in detail in Appendix A. These experiments showed complete cleavage of the peptide after an incubation of 60 min. The SERS spectra of the peptide fragments showed complete disappearance of the F peak as expected, indicating that monitoring the SERS peaks of the aromatic amino acids should allow monitoring trypsin activity.

4.2. SERS spectroscopy on the mixture from an in-solution trypsin cleavage experiment

Secondly, we again performed in-solution cleavage and then immediately labelled gold nanodomes with the solution containing peptide fragments and the protease. In principle, only the peptide fragment containing the N-terminal cysteine should attach to the gold surface of the SERS substrate via a gold-sulfur bond. The SERS spectra of the solution (see Appendix B for more details) indeed showed only the SERS peak of CN-F, indicating that the short peptide fragment, GNFSF, was cleaved off and did not non-specifically attach to the gold surface.

Biomedical Optics EXPRESS

4.3. Labelling gold nanodomes with the intact peptide and performing trypsin cleavage directly on the SERS chip

Last, we checked if the peptide can also be cleaved when attached to the gold surface of the SERS substrate. Therefore, gold nanodomes were first labelled with the peptide, such that a peptide monolayer had formed on the gold surface. This monolayer must provide cleavage sites that are accessible for the protease. Additionally, the gaps of the SERS structures need to be sufficiently big such that they remain accessible to the protease that needs to diffuse to the peptide monolayer in the gaps, where the SERS enhancement is the highest.

We incubated the peptide-labelled nanodomes in three conditions: 1. In ammonium bicarbonate buffer without any trypsin present, to serve as a reference measurement. 2. With trypsin dissolved in ammonium bicarbonate buffer at a concentration of 5 µg/ml. We only expected to observe trypsin activity and the corresponding F peak decrease in this condition. 3. In ammonium bicarbonate buffer with inactivated trypsin. Trypsin (at 5 µg/ml) was inactivated using the inhibitor phenylmethylsulfonyl fluoride (PMSF, 40 µg/ml) [46]. The samples were incubated for 60 min at 37 °C, rinsed and their SERS spectra acquired. The SERS spectra before and after trypsin addition (for condition 2) are shown in Fig. 3. It is evident that trypsin efficiently cleaved the peptide, resulting in a decrease in the intensity of the SERS peak of phenylalanine (F) at 1003 cm^{-1}. We also concluded that this partial F peak decrease can be ascribed to the limited accessibility of the nanodome gaps for trypsin, as established in [16].

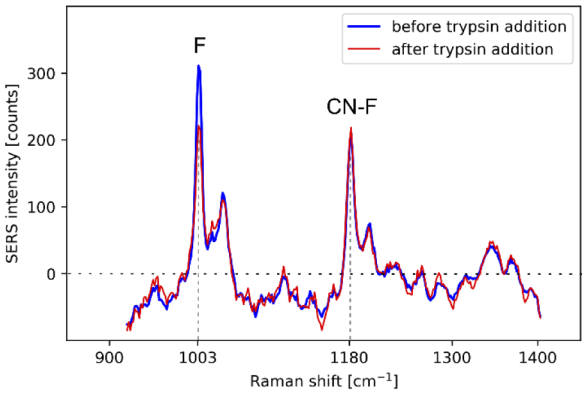

Fig. 3. SERS spectra of the peptide before and after trypsin addition, recorded on gold nanodomes. Addition of trypsin results in a decrease in the intensity of the SERS peak of phenylalanine (F) at 1003 cm^{-1}.

The F/CN-F peak intensities were then calculated for all three different conditions (Fig. 4). We noticed that the 30% decrease in the F/CN-F peak intensity ratio is only caused by trypsin cleavage of the peptide substrate, as no change in the SERS spectra is detected in the presence of inactivated trypsin or when no trypsin is added. We can therefore conclude that the peptide substrate NH_2–CALNN(CN-F)GSG(CN-F)GGGGVRGNFSF-COOH can be labelled on the gold nanodomes and cleaved by trypsin. However, likely due to the limited accessibility of the nanodome gaps for trypsin, this cleavage is not complete.

We have thus shown that SERS can be used to detect trypsin activity on gold nanodomes, using peptide substrates holding non-natural aromatics. Gold nanodomes are however free-space SERS substrates, requiring specialized laboratory equipment for the acquisition of Raman spectra. In the next sections, we therefore explore the use of the integrated nanoplasmonic slot waveguide for SERS detection of protease activity.

Biomedical Optics EXPRESS

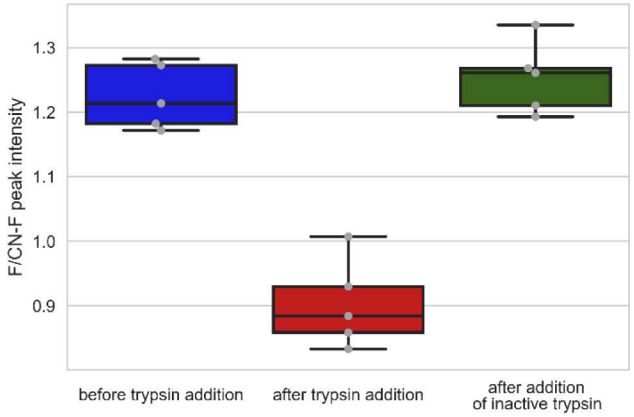

Fig. 4. F/CN-F peak intensity ratio for the trypsin cleavage experiments performed on gold nanodomes. The box plot shows that the F/CN-F peak intensity ratio decreases by 30% after trypsin addition. If no trypsin is added, or after the addition of inactive trypsin, there is no change in the F/CN-F peak intensity ratio.

4.4. Detecting the peptide monolayer on nanoplasmonic slot waveguides

The nanoplasmonic slot waveguide was labelled with the peptide. To acquire the SERS spectra of the nanoplasmonic slot waveguide on the confocal Raman microscope, the sample was positioned vertically, and end-fire coupled [27]. A Zeiss 63×/0.9 EC Epiplan NEOFLUAR:∞/0 objective was used to couple the light into the waveguide with the laser power of 1 mW measured before the microscope objective and the integration time set to 5 s. The estimated laser power that was guided in the waveguide is approximately 300 µW, based on the coupling losses reported in [27]. A raw SERS spectrum is shown in Fig. 5, which shows that the SERS background signal is quite high, but nevertheless the CN-F peak at 1180 cm^{-1} is clearly visible. The peak around 1600 cm^{-1} can be ascribed to the CALNN sequence in the peptide [16] and the peak at 2330 cm^{-1} belongs to the silicon nitride, and therefore indicates that the light is indeed guided in the Si_3N_4 waveguide [19]. The Si_3N_4 is also the main origin of the broad background features [32].

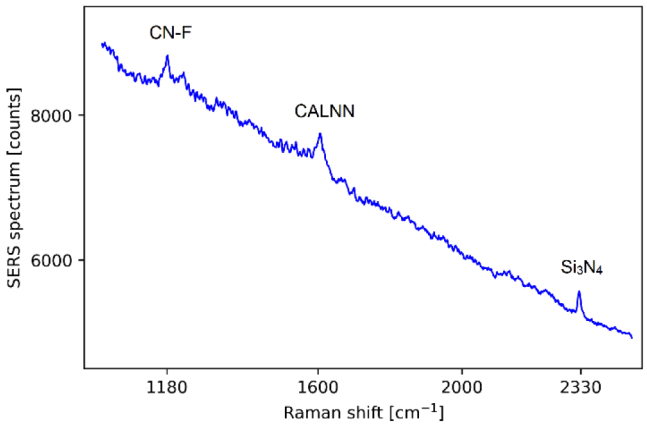

Fig. 5. Raw SERS spectrum of the trypsin peptide substrate acquired on the nanoplasmonic slot waveguide. The silicon nitride peak at 2330 cm^{-1} indicates that the light is guided in the waveguide, whereas the other two peaks originate from the peptide itself. The background originates predominantly from the silicon nitride waveguide.

Biomedical Optics EXPRESS

4.5. Stability of the SERS spectra of the peptide on the nanoplasmonic slot waveguide

When acquiring SERS signals of different Raman reporters, the stability of the SERS spectra needs to be monitored. Upon prolonged exposure to high input laser power, Raman reporters may overheat and potentially burn or experience other chemical transitions that affect their molecular structure and therefore their Raman spectrum. One example is the photoinduced reduction of nitrothiophenol (NTP) to dimercaptoazobenzene, where these chemical changes affect the SERS signal strength of the 1339 cm^{-1} mode of the NTP [47].

In the case of the free-space excited nanodomes, this problem can be avoided by acquiring spectra at several different locations on the nanodome sample. However, when switching to waveguide-based nanoplasmonic slot waveguides, we are limited by the fact that we can excite and collect SERS spectra of one waveguide through only one access point, i.e. the silicon nitride access waveguide. We therefore have to pay special attention to use appropriate laser powers that will not chemically damage the peptides as this could lead to peak intensity changes similar to those caused by the trypsin cleavage of the peptide.

Due to the various parameters such as the coupling efficiency and the length of the access waveguide which can affect the amount of laser light that reaches the peptide [27], we have to ensure the stability of the SERS signal over time for each individual experiment. The nanoplasmonic slot waveguides were therefore fabricated in sets of two, one serving as a reference waveguide, where the stability of the SERS signal of the peptide is established under continuous laser illumination. An example of a reference measurement of the F/CN-F peak intensity vs. time is shown in Fig. 6, where the vertical dashed line indicates the average value of the F/CN-F peak intensity. In our experiments, we have typically used the coupled laser power of 300 µW and an integration time of up to 60 s. In the timeframe of our measurement at the given laser power we do not see any significant deterioration of the SERS signal. After the stability of the SERS signal has been successfully established, the protease activity measurement can be performed on the identical second waveguide.

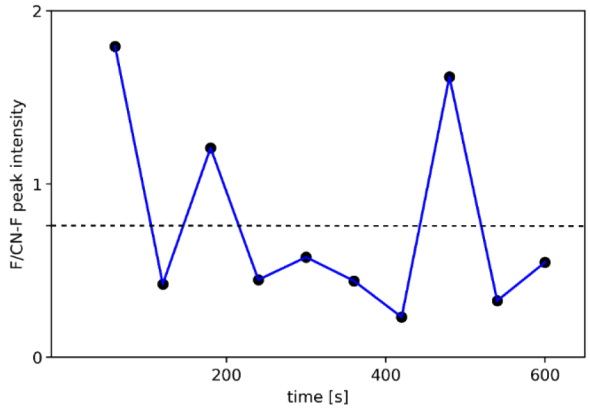

Fig. 6. An example of the F/CN-F peak intensity ratio plot as a function of time obtained on a reference nanoplasmonic slot waveguide. The vertical dashed line indicates the average value of the F/CN-F peak intensity.

4.6. Detection of trypsin activity on the waveguide-based SERS platform

The peptide was labelled on a nanoplasmonic slot waveguide with a gap size of 43 nm. First, the stability of the SERS signal of the peptide under continuous laser illumination was established. After, the SERS spectra of the peptide before and after trypsin incubation were acquired. The SERS substrate was incubated with 5 µg/ml trypsin for 60 min at 37°C. The laser power guided

Biomedical Optics EXPRESS

in the waveguide and used to excite the SERS response was 300 µW, and we recorded 10 measurements for each condition with an integration time of 60 s. In Fig. 7, the averaged spectra of the background-subtracted measurements before and after trypsin addition are presented, showing the disappearance of the F peak, thus indicating trypsin cleavage. To quantify trypsin activity, we calculated the integrated peak counts of the F and CN-F peaks at 1003 cm^{-1} and 1180 cm^{-1}, respectively. We noticed a 70% decrease in the F/CN-F peak intensity upon trypsin incubation as shown in Fig. 8, suggesting that trypsin indeed cleaved the peptide substrate. We again did not notice full disappearance of the signal from the F peak. In this case, the remaining F/CN-F signal could be attributed to another peak that appears at 1010 cm^{-1} after trypsin addition and could thus be considered an artefact of our data analysis. The 43 nm gap of the nanophotonic slot waveguide should namely allow much better accessibility to trypsin compared to the much smaller 12 nm gaps of the gold nanodomes. To achieve higher SERS signal, the smaller gap sizes would however be preferable, if they could still provide sufficient accessibility to the trypsin.

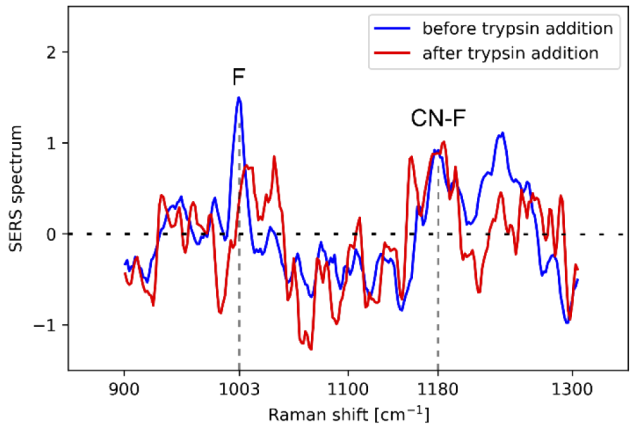

Fig. 7. SERS spectra of the peptide before and after trypsin addition acquired on nanoplasmonic slot waveguide. The decrease in the F peak at 1003 cm^{-1} indicates trypsin-mediated cleavage of the peptide. Each spectrum shown in the graph is the average of 10 background-subtracted measurements. For better visualization, the spectra were smoothed with the simple moving average with the window size of 3.

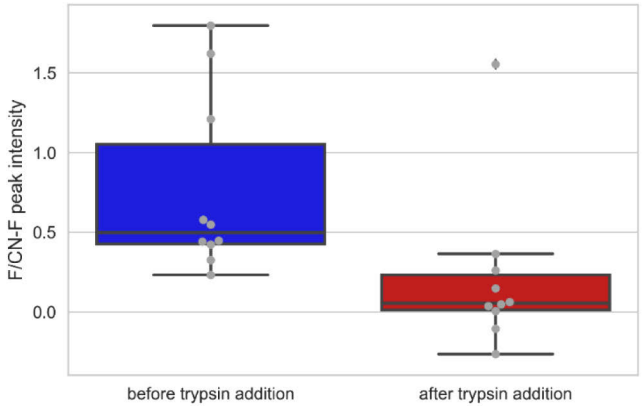

Fig. 8. A box plot of F/CN-F peak intensities before and after trypsin addition recorded on nanoplasmonic slot waveguide. Individual measurements are presented as gray dots.

Biomedical Optics EXPRESS

5. Conclusions

In this proof-of-concept demonstration, we have shown waveguide-based SERS detection of trypsin activity via the cleavage of its peptide substrate that holds non-natural aromatic amino acids. We have demonstrated trypsin activity detection for a trypsin concentration of 2×10^{-7} M, however, it was previously shown that this technique can reach a detection limit of at least 8×10^{-9} M [16]. Whereas there already exist techniques that enable lower detection limits [48,49], the use of the waveguide-based SERS substrate opens the possibility of integration of the SERS sensor on a photonic integrated circuit. By using an integrated approach, different functionalities of a laboratory system, such as lasers, spectrometers, filters and detectors, can be implemented on a small, mass-produced and reliable photonic chip. Such a lab-on-a-chip modality further enables extensive parallelization of measurements. In the last years, the performance of the integrated SERS substrates is continuously improving, yet the waveguide-based SERS substrates currently still do not enable the high SERS enhancements achieved in free-space SERS substrates. To mediate this, we have developed a peptide substrate incorporating non-natural aromatic amino acids, which provide a high intrinsic Raman signal. Since only the three natural aromatics provide relatively strong Raman signals, the use of non-natural aromatics is also crucial for the development of the multiplexing SERS measurements, where the activity of several proteases can be detected at the same time using different, protease-specific peptide substrates with non-overlapping SERS peaks. Using non-natural aromatics significantly expands possibilities of multiplexing, and the non-natural aromatics can additionally provide higher SERS signal strengths than those of the natural aromatics, thus improving the SERS signal-to-noise ratio.

Appendix A

In-solution trypsin cleavage of the peptide monitored via RP-HPLC and SERS spectroscopy

We performed bulk trypsin cleavage of the peptide substrate, separated the peptide fragments by RP-HPLC, labelled them on the gold nanodomes and collected their SERS spectra. First, trypsin was dissolved in 50 mM ammonium bicarbonate buffer (pH = 7.8) to a concentration of 5 µg/ml. The solution was warmed to 37°C, which is the optimal working temperature for trypsin. The lyophilized peptide was in the meantime first dissolved in DMF at a concentration of 25 µg/µl and then added to the trypsin solution in the ammonium bicarbonate buffer to a final peptide concentration of 100 µg/ml and left to incubate for an hour at 37°C. We then separated the peptide solution via RP-HPLC. HPLC chromatograms are shown in Fig. 9 for the intact peptide and Fig. 10 for the peptide incubated with trypsin. We analyzed the collected fractions by means of MALDI-based mass spectrometry to determine the masses of the prominent HPLC peaks, and thus to conclude which peptide (fragment) they represent.

In the chromatogram of the intact peptide, shown in Fig. 9, we see a prominent peak at an elution time of 39.5 min with a mass corresponding to that of the intact peptide monomer. We additionally see a smaller peak eluting around 43 min. MALDI-MS analysis indicate that the peptides in this fraction had the same mass as in the case of the monomer, but it is more likely that this peptide is actually a dimer – as it eluted at a later time point and is thus more hydrophobic – that broke down into two monomers in the mass spectrometer ionization chamber. The peptides we use start with a cysteine and two such cysteines (of thus two individual peptides) can form a sulfur bridge (disulfide bridge) under oxidizing conditions. It has previously been shown that the formation of dimers does not drastically reduce the ability of the peptides to bond to the gold surface that we wish to use as SERS substrates [16].

Figure 10 shows the RP-HPLC analysis of the peptide substrate digested by trypsin. Here, we want to primarily establish that trypsin cleaves its substrate specifically, i.e. only at the arginine (R) cleavage site. Furthermore, we want to determine how long the incubation needs

Biomedical Optics EXPRESS

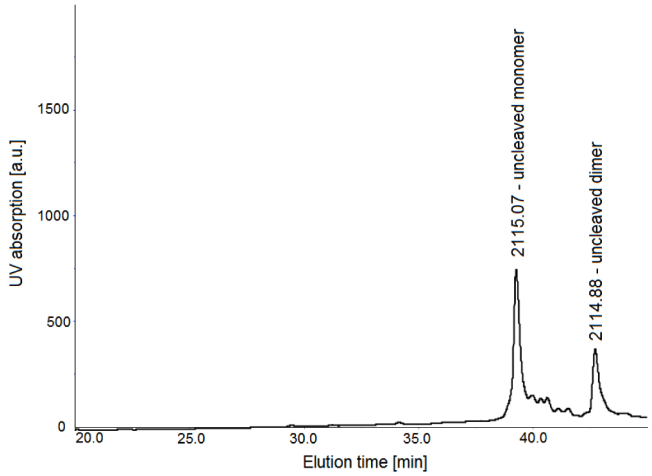

Fig. 9. RP-HPLC chromatogram of the intact peptide (trypsin substrate). The measured mass (in Da) along with the identified peptide fraction is written above each HPLC peak.

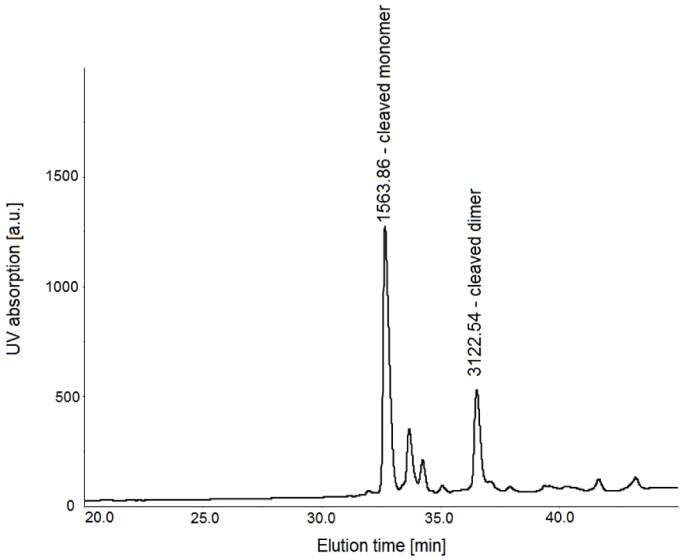

Fig. 10. RP-HPLC chromatogram of the trypsin-digested peptide. The measured mass (in Da) along with the identified peptide fraction is written above each HPLC peak.

Biomedical Optics EXPRESS

to be for complete peptide cleavage in solution. Previous experiments suggested that trypsin cleavage is quite fast and we could expect to see full peptide cleavage after about one hour of incubation [16]. In Fig. 10, we see that the peaks of peptides eluting at 39.5 and 43 min disappear, suggesting that the peptide had been completely digested. Further, two prominent peaks now appear at 33 and 37 min. The masses of the peptides in these peaks correspond to the adducts of the long peptide fragments of the cleaved monomer and the cleaved dimer, namely NH_2-CALNN(CN-F)GSG(CN-F)GGGGVR-COOH, as expected. Adducts are a common occurrence in mass spectroscopy analysis, and stem from the fact that the peptide fragment binds to a sodium or potassium ion, resulting in a corresponding increase in the mass of the peptide ion.

After establishing that the peptide was cleaved specifically and fully by trypsin, we labelled the gold nanodomes with the collected HPLC fractions to collect their SERS spectra. The gold nanodomes were cleaned with acetone, isopropyl alcohol and deionized (DI) water, and dried with a N_2 gun. After placing the gold nanodomes in oxygen plasma for 2 min, the nanodomes were immersed overnight in the peptide solutions and rinsed with DI water to remove peptides that did not covalently bind to the gold surface. The samples were placed in a Petri dish filled with 3 ml of 50 mM ammonium bicarbonate buffer (pH 7.8). The SERS spectra of the peptides were acquired with the WITec confocal Raman microscope. For gold nanodomes, a 1 mW laser power before the microscope objective and a 40x/0.5 Zeiss water immersion objective were used to acquire spectra on a spatially distributed map of 7×7 pixels in a 40×40 µm area with an integration time of 3 s on each point to avoid signal degradation upon laser illumination.

Starting from 7×7 individual spectra, cosmic rays were removed using WITec Project Four. The data were then exported to MATLAB and deviant spectra were discarded using a variance-based filter. Then, the background of each individual spectrum was subtracted using a high-pass filter. Each SERS spectrum, which was acquired on gold nanodomes, is the average spectra of these data. In Fig. 11, the SERS spectra of different peptides or peptide fragments are plotted, normalized on the CN-F maximum peak intensity.

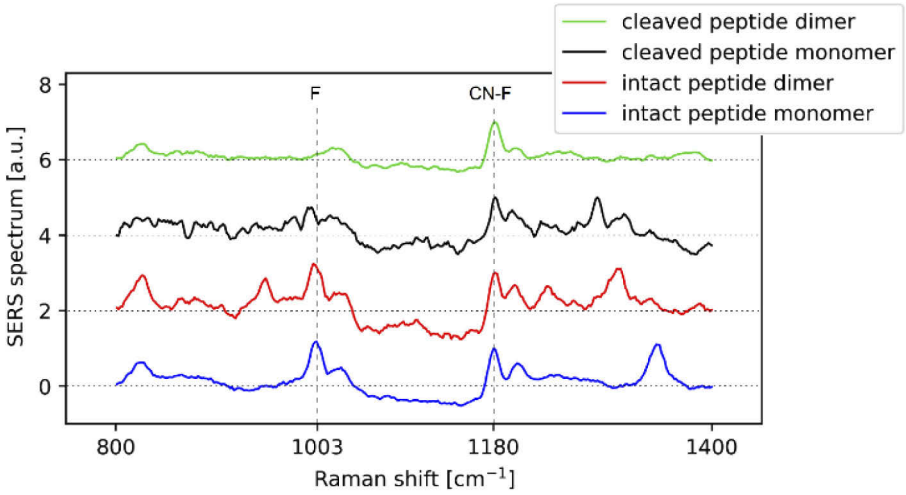

Fig. 11. SERS spectra of the RP-HPLC separated peptides from a bulk trypsin cleavage experiment. The spectra are normalized on the CN-F maximum peak intensity for easier comparison and offset on the y axis. The horizontal vertical lines represent the zero of each spectrum. The two vertical lines represent the positions of the characteristic SERS peaks of the phenylalanine (F) and 4-cyano-phenylalanine (CN-F). After trypsin digestion, a complete disappearance of the SERS peak of phenylalanine F is evident, as expected.

Biomedical Optics EXPRESS

We found that the gold nanodomes labelled with both the intact peptide monomer and dimer display the two characteristic SERS peaks, one at 1003 cm^{-1} corresponding to phenylalanine (F) and another at 1180 cm^{-1} that can be ascribed to 4-cyano-phenylalanine (CN-F). As indicated above, also the peptide dimer seems to efficiently attach to the gold SERS substrate. After trypsin cleavage of the peptide substrate, the F peak completely disappears, as expected. We can therefore conclude that monitoring the SERS peaks of the aromatic amino acids is a suitable metric for monitoring the trypsin activity.

Appendix B

SERS spectroscopy analysis of the in-solution trypsin cleavage experiment

As the next control experiment, we again performed bulk cleavage of the peptide with trypsin, exactly as described in the previous section. We then immediately labelled the gold nanodomes with the cleavage solution containing the mix of all peptide fragments. In principle, only the long peptide fragment should be able to bind to the gold surface via a sulfur-gold bond via its N-terminal cysteine. We expect that the short peptide fragment, NH_2-GNFSF-COOH, would be washed away from the gold surface when rinsing the gold nanodomes after overnight labelling. We recorded SERS spectra from gold nanodomes labelled with the peptide solution using the same acquisition parameters as in Appendix A. The SERS spectra are shown in Fig. 12 and were normalized on the CN-F peak at 1180 cm^{-1} for easier comparison.

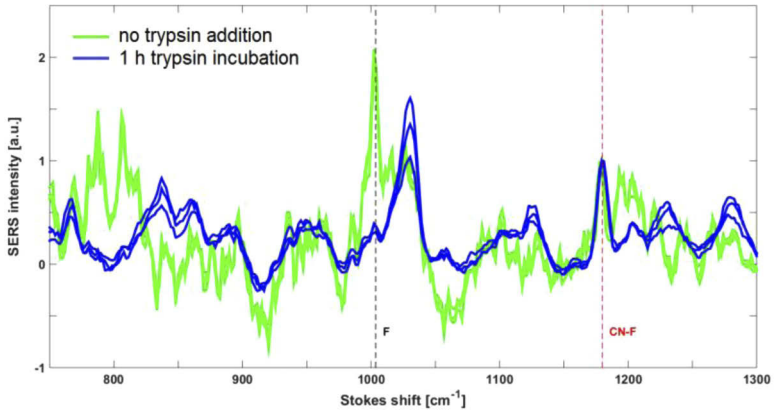

Fig. 12. SERS spectra of the intact peptide (green) and of the cleavage solution after 1 h of incubating the peptide with trypsin (blue). The three spectra for each condition come from three different gold nanodome samples, all labelled under the same conditions. All spectra are normalized on the CN-F peak at 1180 cm^{-1}.

We can see that the F peak disappears completely as expected after trypsin incubation, showing full cleavage of the peptide. To quantify this, we calculated the ratio of the SERS peak intensities by integrating the F and CN-F peak counts at their respective positions and subtracting the background with a linear fit for the individual spectra. We used the F/CN-F peak intensity ratio as a metric for the (efficiency of) trypsin cleavage, as plotted in Fig. 13. As can be seen, due to the disappearance of the F peak, the F/CN-F peak intensity is greatly reduced upon trypsin digestion. Based on the experiments in the previous section showing complete cleavage of the peptide substrate, the small remaining contribution of the F peak after trypsin incubation can be ascribed to the data analysis method used and not to the contribution of the remains of uncleaved peptide.

Biomedical Optics EXPRESS

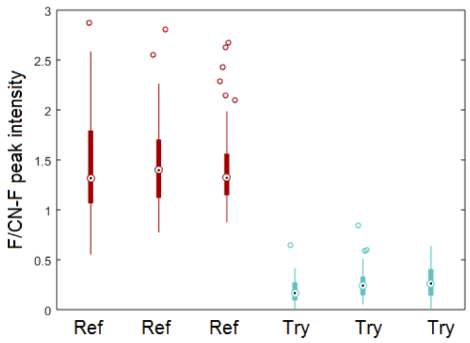

Fig. 13. A box plot of F/CN-F peak intensities before (Ref) and after (Try) trypsin addition for the spectra shown in Fig. 12. Each box plot corresponds to one SERS spectrum in the previous figure.

Funding

Fonds Wetenschappelijk Onderzoek (1179319N); Methusalem grant; Bijzonder Onderzoeksfonds UGent.

Acknowledgements

The authors thank Dieter Cuypers for performing the gold deposition and Liesbet Van Landschoot for taking the SEM pictures.

Disclosures

The authors declare no competing financial interest.

References

1. M. Drag and G. S. Salvesen, "Emerging principles in protease-based drug discovery," Nat. Rev. Drug Discovery **9**(9), 690–701 (2010).
2. B. Turk, "Targeting proteases: successes, failures and future prospects," Nat. Rev. Drug Discovery **5**(9), 785–799 (2006).
3. C. G. Smith and J. R. Vane, "The Discovery of Captopril," FASEB J. **17**(8), 788–789 (2003).
4. C. Flexner, G. Bate, and P. Kirkpatrick, "Tripnavir," Nat. Rev. Drug Discovery **4**(12), 955–956 (2005).
5. I. M. Verhamme, S. E. Leonard, and R. C. Perkins, "Proteases: Pivot Points in Functional Proteomics," in *Functional Proteomics Methods and Protocols*, 313–392 (Humana Press, New York, 2018).
6. W. F. Patton, "Detection technologies in proteome analysis," J. Chromatogr. B: Anal. Technol. Biomed. Life Sci. **771**(1-2), 3–31 (2002).
7. I. L. H. Ong and K.-L. Yang, "Recent developments in protease activity assays and sensors," Analyst **142**(11), 1867–1881 (2017).
8. K. Welser, R. Adsley, B. M. Moore, W. C. Chan, and J. W. Aylott, "Protease sensing with nanoparticle based platforms," Analyst **136**(1), 29–41 (2011).
9. Y. Lai, S. Sun, T. He, S. Schlücker, and Y. Wang, "Raman-encoded microbeads for spectral multiplexing with SERS detection," RSC Adv. **5**(18), 13762–13767 (2015).
10. M. Moskovits, "Surface-enhanced spectroscopy," Rev. Mod. Phys. **57**(3), 783–826 (1985).
11. L. Chen, X. Fu, and J. Li, "Ultrasensitive surface-enhanced Raman scattering detection of trypsin based on anti-aggregation of 4-mercaptopyridine-functionalized silver nanoparticles: an optical sensing platform toward proteases," Nanoscale **5**(13), 5905–5911 (2013).
12. Z. Wu, Y. Liu, X. Zhou, A. Shen, and J. Hu, "A "turn-off" SERS-based detection platform for ultrasensitive detection of thrombin based on enzymatic assays," Biosens. Bioelectron. **44**, 10–15 (2013).
13. Z. Wu, Y. Liu, Y. Liu, H. Xiao, A. Shen, X. Zhou, and J. Hu, "A simple and universal "turn-on" detection platform for proteases based on surface enhanced Raman scattering (SERS)," Biosens. Bioelectron. **65**, 375–381 (2015).
14. A. N. Ramya, M. M. Joseph, J. B. Nair, V. Karunakaran, N. Narayanan, and K. K. Maiti, "New Insight of Tetraphenylethylene-based Raman Signatures for Targeted SERS Nanoprobe Construction Toward Prostate Cancer Cell Detection," ACS Appl. Mater. Interfaces **8**(16), 10220–10225 (2016).

Biomedical Optics EXPRESS

15. C. Sun, K.-H. Su, J. Valentine, Y. T. Rosa-Bauza, J. A. Ellman, O. Elboudwarej, B. Mukherjee, C. S. Craik, M. A. Shuman, F. F. Chen, and X. Zhang, "Time-Resolved Single-Step Protease Activity Quantification Using Nanoplasmonic Resonator Sensors," ACS Nano **4**(2), 978–984 (2010).
16. P. C. Wuytens, H. Demol, N. Turk, K. Gevaert, A. Skirtach, M. Lamkanfi, and R. Baets, "Gold nanodome SERS platform for label-free detection of protease activity," Faraday Discuss. **205**, 345–361 (2017).
17. E. Le Ru and P. Etchegoin, *Principles of Surface-Enhanced Raman Spectroscopy*, Elsevier Science (2008).
18. A. Z. Subramanian, E. Ryckeboer, A. Dhakal, F. Peyskens, A. Malik, B. Kuyken, H. Zhao, S. Pathak, A. Ruocco, A. D. Groote, P. Wuytens, D. Martens, F. Leo, W. Xie, U. D. Dave, M. Muneeb, P. V. Dorpe, J. V. Campenhout, W. Bogaerts, P. Bienstman, N. L. Thomas, D. V. Thourhout, Z. Hens, G. Roelkens, and R. Baets, "Silicon and silicon nitride photonic circuits forspectroscopic sensing on-a-chip," Photonics Res. **3**(5), B47–B59 (2015).
19. A. Dhakal, A. Z. Subramanian, P. Wuytens, F. Peyskens, N. Le Thomas, and R. Baets, "Evanescent excitation and collection of spontaneous Raman spectra using silicon nitride nanophotonic waveguides," Opt. Lett. **39**(13), 4025–4028 (2014).
20. A. Dhakal, A. Raza, F. Peyskens, A. Z. Subramanian, S. Clemmen, N. Le Thomas, and R. Baets, "Efficiency of evanescent excitation and collection of spontaneous Raman scattering near high index contrast channel waveguides," Opt. Express **23**(21), 27391–27404 (2015).
21. S. A. Holmstrom, T. H. Stievater, D. A. Kozak, M. W. Pruessner, N. Tyndall, W. S. Rabinovich, R. A. McGill, and J. B. Khurgin, "Trace gas Raman spectroscopy using functionalized waveguides," Optica **3**(8), 891–896 (2016).
22. D. M. Kita, J. Michon, and J. Hu, "A packaged, fiber-coupled waveguide-enhanced Raman spectroscopic sensor," Opt. Express **28**(10), 14963–14972 (2020).
23. F. Peyskens, A. Dhakal, P. Van Dorpe, N. Le Thomas, and R. Baets, "Surface Enhanced Raman Spectroscopy Using a Single Mode Nanophotonic-Plasmonic Platform," ACS Photonics **3**(1), 102–108 (2016).
24. F. Tang, P.-M. Adam, and S. Boutami, "Theoretical investigation of SERS nanosensors based on hybrid waveguides made of metallic slots and dielectric strips," Opt. Express **24**(19), 21244–21255 (2016).
25. P. C. Wuytens, A. G. Skirtach, and R. Baets, "On-Chip Surface-Enhanced Raman Spectroscopy using Nanosphere-Lithography Patterned Antennas on Silicon Nitride Waveguides," Opt. Express **25**(11), 12926–12934 (2017).
26. F. Peyskens, P. Wuytens, A. Raza, P. Van Dorpe, and R. Baets, "Waveguide excitation and collection of surface-enhanced Raman scattering from a single plasmonic antenna," Nanophotonics **7**(7), 1299–1306 (2018).
27. A. Raza, S. Clemmen, P. Wuytens, M. Muneeb, M. Van Daele, J. Dendooven, C. Detavernier, A. Skirtach, and R. Baets, "ALD assisted nanoplasmonic slot waveguide for on-chip Enhanced Raman Spectroscopy," APL Photonics **3**(11), 116105 (2018).
28. H. M. K. Wong, M. K. Dezfouli, L. Sun, S. Hughes, and A. S. Helmy, "Nanoscale Plasmonic Slot Waveguides for Enhanced Raman Spectroscopy," Phys. Rev. B **98**(8), 085124 (2018).
29. Q. Cao, J. Feng, H. Lu, H. Zhang, F. Zhang, and H. Zeng, "Surface-enhanced Raman scattering using nanoporous gold on suspended silicon nitride waveguides," Opt. Express **26**(19), 24614–24620 (2018).
30. S. Li, L. Xia, X. Chen, Z. Yang, and W. Li, "Surface-enhanced Raman scattering sensor based on hybrid deep slot waveguide on an integrated photonic platform," J. Opt. Soc. Am. B **36**(9), 2423–2428 (2019).
31. S. Li, L. Xia, Z. Yang, M. Zhou, B. Zhao, and W. Li, "Hybrid plasmonic grating slot waveguide with high field enhancement for an on-chip surface-enhanced Raman scattering sensor," Appl. Opt. **59**(3), 748–755 (2020).
32. A. Dhakal, P. Wuytens, A. Raza, N. Le Thomas, and R. Baets, "Silicon Nitride Background in Nanophotonic Waveguide Enhanced Raman Spectroscopy," Materials **10**(2), 140 (2017).
33. A. Raza, S. Clemmen, P. Wuytens, M. de Goede, A. S. K. Tong, N. Le Thomas, C. Liu, J. Suntivich, A. G. Skirtach, S. M. Garcia-Blanco, D. J. Blumenthal, J. S. Wilkinson, and R. Baets, "High index contrast photonic platforms for on-chip Raman spectroscopy," Opt. Express **27**(16), 23067–23079 (2019).
34. N. Turk, A. Raza, P. Wuytens, H. Demol, M. Van Daele, C. Detavernier, A. Skirtach, K. Gevaert, and R. Baets, "Comparison of Free-Space and Waveguide-Based SERS Platforms," Nanomaterials **9**(10), 1401 (2019).
35. A. Dhakal, C. Wuytens, F. Peyskens, K. Jans, N. Le Thomas, and R. Baets, "Nanophotonic waveguide enhanced Raman spectroscopy of biological submonolayers," ACS Photonics **3**(11), 2141–2149 (2016).
36. G. Zhu, X. Zhu, Q. Fan, and X. Wan, "Raman spectra of amino acids and their aqueous solutions," Spectrochim. Acta, Part A **78**(3), 1187–1195 (2011).
37. C. L. Weeks, A. Polishchuk, Z. Getahun, W. F. DeGrado, and T. G. Spiro, "Investigation of an unnatural amino acid for use as a resonance Raman probe: Detection limits, solvent and temperature dependence of the νC≡N band of 4-cyanophenylalanine," J. Raman Spectrosc. **39**(11), 1606–1613 (2008).
38. F. Wei, D. Zhang, N. J. Halas, and J. D. Hartgerink, "Aromatic Amino Acids Providing Characteristic Motifs in the Raman and SERS Spectroscopy of Peptides," J. Phys. Chem. B **112**(30), 9158–9164 (2008).
39. H. Häkkinen, "The gold-sulfur interface at the nanoscale," Nat. Chem. **4**(6), 443–455 (2012).
40. R. Lévy, N. T. K. Thanh, R. C. Doty, I. Hussain, R. J. Nichols, D. J. Schiffrin, M. Brust, and D. G. Fernig, "Rational and Combinatorial Design of Peptide Capping Ligands for Gold Nanoparticles," J. Am. Chem. Soc. **126**(32), 10076–10084 (2004).
41. E. Vandermarliere, M. Michael, and M. Lennart, "Getting intimate with trypsin, the leading protease in proteomics," Mass Spectrom. Rev. **32**(6), 453–465 (2013).
42. H. P. Erickson, "Size and Shape of Protein Molecules at the Nanometer Level Determined by Sedimentation, Gel Filtration, and Electron Microscopy," Biol. Proced. Online **11**(1), 32–51 (2009).

Biomedical Optics EXPRESS

43. E. P. Haglund, S. Kumari, P. Westbergh, J. S. Gustavsson, G. Roelkens, R. Baets, and A. Larsson, "Silicon-integrated short-wavelength hybrid-cavity VCSEL," Opt. Express **23**(26), 33634–33640 (2015).
44. X. Nie, N. Turk, Y. Li, Z. Liu, and R. Baets, "High extinction ratio on-chip pump-rejection filter based on cascaded grating-assisted contra-directional couplers in silicon nitride rib waveguides," Opt. Lett. **44**(9), 2310–2313 (2019).
45. X. Nie, E. Ryckeboer, G. Roelkens, and R. Baets, "CMOS-compatible broadband co-propagative stationary Fourier transform spectrometer integrated on a silicon nitride photonics platform," Opt. Express **25**(8), A409–A418 (2017).
46. J. C. Powers, J. L. Asgian, Ö. Doğan Ekici, and K. Ellis James, "Irreversible Inhibitors of Serine, Cysteine, and Threonine Proteases," Chem. Rev. **102**(12), 4639–4750 (2002).
47. M. Tabatabaei, A. Sangar, N. Kazemi-Zanjani, P. Torchio, A. Merlen, and F. Lagugné-Labarthet, "Optical Properties of Silver and Gold Tetrahedral Nanopyramid Arrays Prepared by Nanosphere Lithography," J. Phys. Chem. C **117**(28), 14778–14786 (2013).
48. E. Gizem, M. Hedström, and B. Mattiasson, "A sensitive and real-time assay of trypsin by using molecular imprinting-based capacitive biosensor," Biosens. Bioelectron. **86**, 557–565 (2016).
49. L. Hu, S. Han, S. Parveen, Y. Yuan, L. Zhang, and G. Xua, "Highly sensitive fluorescent detection of trypsin based on BSA-stabilized gold nanoclusters," Biosens. Bioelectron. **32**(1), 297–299 (2012).